

Structure-guided development of affinity probes for tyrosine kinases using chemical genetics

Jimmy A Blair^{1,2}, Daniel Rauh², Charles Kung², Cai-Hong Yun^{3,4}, Qi-Wen Fan⁵, Haridas Rode⁶, Chao Zhang², Michael J Eck^{3,4}, William A Weiss⁵ & Kevan M Shokat^{1,2}

As key components in nearly every signal transduction pathway, protein kinases are attractive targets for the regulation of cellular signaling by small-molecule inhibitors. We report the structure-guided development of 6-acrylamido-4-anilinoquinazoline irreversible kinase inhibitors that potently and selectively target rationally designed kinases bearing two selectivity elements that are not found together in any wild-type kinase: an electrophile-targeted cysteine residue and a glycine gatekeeper residue. Cocrystal structures of two irreversible quinazoline inhibitors bound to either epidermal growth factor receptor (EGFR) or engineered c-Src show covalent inhibitor binding to the targeted cysteine (Cys797 in EGFR and Cys345 in engineered c-Src). To accommodate the new covalent bond, the quinazoline core adopts positions that are different from those seen in kinase structures with reversible quinazoline inhibitors. Based on these structures, we developed a fluorescent 6-acrylamido-4-anilinoquinazoline affinity probe to report the fraction of kinase necessary for cellular signaling, and we used these reagents to quantitate the relationship between EGFR stimulation by EGF and its downstream outputs—Akt, Erk1 and Erk2.

Owing to the conserved structural elements of protein kinases and the dynamic nature of kinase cascades, the study of cellular signaling remains a challenge. A variety of powerful methods (for example, gene knockouts, RNA interference and pharmacological agents) are available for determining the role of kinases within signaling cascades. Pharmacological agents such as small organic molecules are particularly powerful because they offer rapid and dose-dependent control over kinase activity. However, two key issues arise when interpreting the cellular effects of kinase inhibition by small molecules. First, few (if any) ATP-competitive kinase inhibitors are truly specific for a single kinase because key structural elements of the active site across all 518 human kinases are conserved; off-target effects are common^{1,2}. Second, the intracellular concentration and biological activity of kinase inhibitors are both greatly influenced by multiple factors, including barriers to cell permeability, drug efflux, cellular metabolism, competition with ATP, and the presence of cellular phosphatases, the endogenous antagonists of kinase activity^{2,3}. Genetic techniques offer a potential solution to these issues because knockouts result in complete loss of the protein kinase (100% inhibition), yet cellular compensation often confounds the analysis of highly adaptive pathways^{2,4}. Thus, although typical small-molecule kinase inhibitors allow rapid and dose-dependent inhibition of kinases inside a cell, current technology does not provide a quantitative understanding of how the

degree of kinase activity relates to cellular function. By addressing this problem, we seek to identify the consequences of partial kinase inhibition, with the hope of identifying the most pharmacologically sensitive nodes within a signaling cascade. To achieve this, it is critical to inhibit a single kinase and to quantitate the degree of inhibition achieved *in vivo*.

To develop an active site affinity probe capable of measuring inhibitor occupancy, we took design cues from the field of activity-based probes (ABPs). The widespread utility of ABPs demonstrates that irreversible inhibitors provide powerful platforms for measuring the fraction of an enzyme in its active versus its inactive conformation within cells and in cell lysates; ABPs for several protein and lipid kinases have been developed^{5–9}. In particular, wortmannin (**1**), an irreversible inhibitor targeting the catalytic lysine in the phosphatidylinositol-3-OH kinase (PI(3)K) and PI(3)K-related families, has been derivatized with a biotin label; this wortmannin analog demonstrates kinase activity-dependent labeling of DNA-dependent protein kinase (DNA-PK)⁷. Following the design paradigm of ABPs that involves linking reporter groups to reactive substituents, we sought to design an irreversible, inhibitor-based probe incorporating a functional handle for signal readout. Whereas ABPs classically rely on the polyspecificity of a probe to target an enzyme family, we instead designed our affinity probe to label a single targeted kinase.

¹Department of Chemistry, University of California, Berkeley, Berkeley, California 94720, USA. ²Howard Hughes Medical Institute and Department of Cellular and Molecular Pharmacology, University of California, San Francisco, 600 16th Street, MC 2280, San Francisco, California 94158, USA. ³Department of Biological Chemistry and Molecular Pharmacology, Harvard Medical School, Boston, Massachusetts 02115, USA. ⁴Department of Cancer Biology, Dana-Farber Cancer Institute, 44 Binney Street, Boston, Massachusetts 02115, USA. ⁵Departments of Neurology, Neurological Surgery and Pediatrics, and the Brain Tumor Research Center, University of California, San Francisco, San Francisco, California 94143, USA. ⁶Chemical Genomics Centre of the Max Planck Society, Otto-Hahn-Strasse 15, D-44227 Dortmund, Germany. Present addresses: Chemical Genomics Centre of the Max Planck Society, Otto-Hahn-Strasse 15, D-44227 Dortmund, Germany (D.R.) and Novartis Institutes of Biomedical Research, 250 Massachusetts Avenue, Cambridge, Massachusetts 02139, USA (C.K.). Correspondence should be addressed to K.M.S. (shokat@cmp.ucsf.edu).

Received 2 October 2006; accepted 5 February 2007; published online 4 March 2007; doi:10.1038/nchembio866

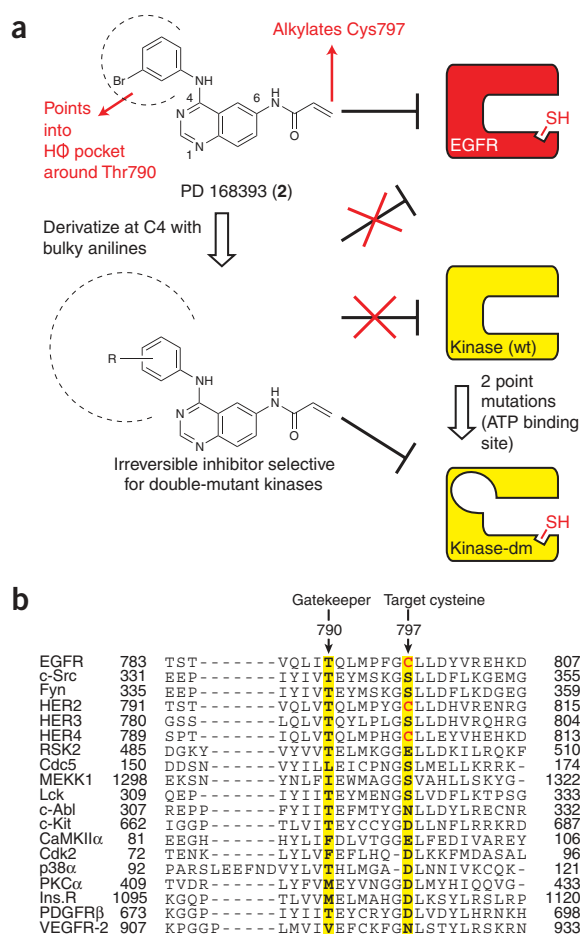


Figure 1 A chemical genetic strategy sensitizes kinases to irreversible inhibitors that do not inhibit wild-type kinases. **(a)** Features of EGFR-selective irreversible inhibitor PD 168393 (**2**) are shown¹³. H_q, hydrophobic. Analysis of kinase cocrystal structures in complex with quinazoline inhibitors suggests that inhibitor derivatives of PD 168393 enlarged at C4 cannot bind to wild-type (wt) kinases because of their increased steric bulk. A double-mutant kinase is sensitized to these inhibitor analogs because of two structural selectivity elements: a smaller gatekeeper and an engineered cysteine analogous to the one targeted in EGFR. **(b)** A partial structure-based sequence alignment of several protein kinases with EGFR¹¹. Residue Thr790 of EGFR is the gatekeeper residue, and Cys797 in EGFR¹³ is targeted for alkylation by PD 168393. A cysteine in this position is conserved among three of the four EGFR-family kinases (conserved cysteines colored in red).

To this end, we developed a general chemical genetic strategy using both inhibitor design and protein kinase engineering. By introducing two rationally designed mutations into the kinase active site, we sensitized two cytoplasmic kinases and a receptor tyrosine kinase (Fyn, c-Src and EGFR) to irreversible chemical inhibitors and a fluorescent affinity probe. First, we mutated the active site ‘gatekeeper’ residue, which is often conserved as a large hydrophobic residue across all protein kinases, to a smaller glycine residue^{10,11}. The resulting expanded binding pocket acts as a selectivity element: it permits binding of kinase inhibitor analogs derivatized with bulky aryl substituents that are sterically occluded from wild-type active sites¹². The second mutation, a cysteine residue that we introduced at the lip of the ATP binding site, serves as an irreversible anchor point for the kinase inhibitor. This facilitates quantitative measurement of active

site occupancy by the inhibitor after cell lysis. Using the quinazoline scaffold of the irreversible EGFR inhibitor PD 168393 (**2**), which reacts with the targeted Cys797 (Cys773 in an alternative numbering scheme) in EGFR¹³, we designed analogs of PD 168393 that bind only kinases containing both a glycine gatekeeper residue and a cysteine residue at the position corresponding to Cys797 in EGFR. To reveal the relative contribution of the dual specificity-determining mutations to the inhibitor binding mode, we solved several cocrystal structures of irreversible inhibitors bound to both EGFR kinase and a second kinase—c-Src kinase containing the electrophile-targeted cysteine mutation. These cocrystal structures of inhibitors irreversibly bound to protein kinases afford us the opportunity to contrast the mode of irreversible inhibitor binding with the wealth of data available from reversible kinase inhibitors. These structures reveal a surprising plasticity in the quinazoline core’s binding to the two different kinases. Based on these structures, we synthesized an irreversible fluorescent affinity probe designed to covalently label an engineered EGFR mutant; we used the probe to measure the fraction of EGFR active sites available for signaling after inhibitor treatment. Subsequent measurement of the phosphorylation of EGFR signaling partners allowed for the correlation of cellular receptor activity with downstream outputs. This chemical genetic strategy enables measurement of the contribution of a kinase to a downstream signaling event.

RESULTS

Design of irreversible inhibitors

Highly specific irreversible kinase inhibitors have been developed against both the EGFR kinase and ribosomal S6 kinase (RSK) families through both optimization of reversible binding and targeting of rare cysteine residues in these two families^{13–15}. These examples served as templates for our chemical genetic strategy. Specifically, we chose as the starting point for inhibitor design the 6-acrylamide-substituted 4-anilinoquinazoline PD 168393, a potent and specific irreversible inhibitor of EGFR and human EGF receptor 2 (HER-2) that reacts with a critical cysteine (Cys797) in the ATP binding site of EGFR (**Fig. 1a**)¹³. Despite the high sequence homology of kinase active sites, a cysteine in a position analogous to Cys797 in EGFR is rare among protein kinases (**Fig. 1b**)¹⁴. A crystal structure of EGFR in complex with erlotinib (**3**; **Fig. 2a**), a reversible 4-anilinoquinazoline similar to PD 168393, shows that the C4 aryl substituent of erlotinib points into a hydrophobic pocket adjacent to Thr790, the gatekeeper residue in EGFR^{16,17}. This binding mode suggests that the 4-anilinoquinazoline might afford an allele-specific kinase inhibitor scaffold. We sought to determine whether, by introducing a cysteine residue at the position corresponding to Cys797 of EGFR into a kinase of choice, we could engineer a second, covalently reactive specificity-determining element.

Synthesis of a panel of inhibitors

We synthesized a small panel of inhibitors using a method previously described for the synthesis of PD 168393 (**Fig. 2a** and **Supplementary Methods** online)¹⁸. The panel included 11 analogs (**2, 4–13**) with C4 substituents of varying steric demand intended to orient into the space occupied by the gatekeeper residue. Detailed synthetic procedures are described in **Supplementary Methods**.

Mutant c-Src generation and irreversible inhibitor screening

Cytoplasmic tyrosine kinases seemed like a tractable target for evaluating the feasibility and extensibility of our chemical genetic design, given their extensive kinetic characterization, their recently reported high-level heterologous expression in bacteria and their proven amenability to analog-sensitive chemical genetics. Therefore,

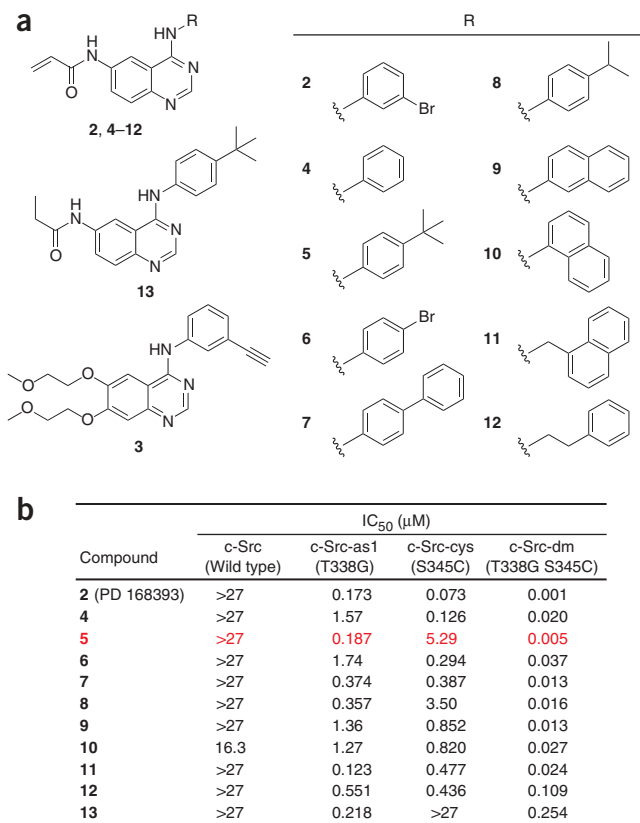


Figure 2 The screening of a panel of C4-derivatized PD 168393 analogs reveals potent, selective inhibitors for an engineered double mutant of c-Src kinase. **(a)** Structures of irreversible inhibitors (**2**, **4–12**) and a reversible inhibitor (**13**) are shown. Erlotinib (**3**), a reversible EGFR inhibitor instrumental in the structure-guided design reported here, is shown for reference. Detailed synthetic methods are described and illustrated in the **Supplementary Methods**. **(b)** IC₅₀ values (in μM) for a panel of inhibitors against c-Src, c-Src-as1, c-Src-cys and c-Src-dm. Inhibitor **5** (highlighted in red text) demonstrates the best balance of potency and selectivity for c-Src-dm.

we introduced cysteine mutations into the cytoplasmic tyrosine kinase c-Src. We previously identified c-Src-as1 (T338G) as an analog-sensitive kinase (an “as-allele”)¹², and alignment of chicken c-Src with EGFR (**Fig. 1b**) identified Ser345 as the candidate for cysteine mutation¹¹. Given that cysteine is isosteric with serine, we hypothesized that this conservative serine-to-cysteine mutation would be functionally silent. We generated a c-Src double mutant (c-Src-dm) that contained T338G and S345C. To investigate the contribution of the cysteine residue alone, we also generated the single cysteine mutant c-Src S345C (c-Src-cys). We expressed the c-Src kinases using a recently reported high-yielding bacterial expression system for tyrosine kinases¹⁹.

Profiling the panel of inhibitors (**2**, **4–13**) against the four c-Src variants revealed substantial structure-activity relationship (SAR) trends (**Fig. 2b**). Though the quinazoline scaffold has been elaborated to give potent, highly selective reversible c-Src inhibitors²⁰, most of the inhibitors described here showed no inhibitory activity against wild-type c-Src at a concentration of 27 μM (**Fig. 2b**), which suggests that the quinazoline scaffold alone does not bind c-Src preferentially and that larger C4 modifications occlude the inhibitors from the wild-type

kinase, as anticipated. Additionally, each inhibitor is substantially more potent against the analog-sensitive mutants c-Src-as1 and c-Src-dm than against wild-type c-Src, which suggests that the gatekeeper residue is a specificity-determining element in the context of C4-derivatized 6-acrylamido-4-anilinoquinazolines. Inhibitors bearing a 6-acrylamide substituent show increased potency for kinases with a targeted cysteine relative to kinases without one, which suggests that irreversible binding occurs, thereby boosting inhibitor potency. Notably, the significant increase in potency of the irreversible inhibitors for c-Src-cys versus c-Src suggests that covalent binding is possible even when the reversible binding mode is non-optimal. Also of note, the reversible inhibitor **13** does not distinguish between cysteine-containing and non-cysteine-containing c-Src variants. Collectively, these results affirm our rational structure-based design of this inhibitor series.

Within this series, inhibitor **5** stands out as the optimal rationally designed inhibitor. A handful of endogenous kinases have a targeted cysteine (for example, EGFR-family kinases), and an important element in the design of covalent inhibitors is to limit potency against these potential native kinases; compound **5** has the least potency against c-Src-cys (half-maximal inhibitory concentration (IC₅₀) = 5.29 μM). Furthermore, **5** is a potent inhibitor of the engineered double mutant, with an IC₅₀ value of 5 nM. These data suggest that **5**, owing to its C4 *p-t*-butylaniline moiety, is especially sensitive to the gatekeeper mutation in the context of a properly positioned cysteine; this inhibitor demonstrates the best balance of selectivity and potency. Screening these inhibitors against Fyn variants, we found similar SAR data for the tyrosine kinase Fyn-dm, which suggests that this chemical genetic strategy may be extensible to other tyrosine kinases (**Supplementary Table 1** online).

Mutant c-Src adducts suggest Cys345-targeted inhibition

Mass spectrometry (ESI-*oa*-TOF) measurements of irreversible inhibitor-treated c-Src mutants were consistent with irreversible inhibition. The single-cysteine mutant, c-Src-cys, treated with **4** had a mass 291 Da higher than that of the control-treated kinase, a result consistent with a 1:1 drug–protein complex (**Fig. 3**). Similarly, the respective masses of c-Src-dm treated with **4** and **5** both correspond to 1:1 adducts. We observed ~30% conversion of c-Src-cys to its inhibitor-kinase adduct when treated with **5**, which is consistent with the lower potency of **5** against kinases with a large gatekeeper. Our attempts to confirm specific alkylation of Cys345 in c-Src-cys and c-Src-dm using proteolysis and tandem mass spectrometry failed, presumably because of poor ionization of the peptide adduct (data not shown). We did not observe alkylation of wild-type c-Src treated with either **4** or **5** (**Fig. 3**), which suggests that irreversible inhibition requires the presence of Cys345.

Complex structures of EGFR

To examine the binding mode of 6-acrylamido-4-anilinoquinazoline inhibitors, we solved the cocrystal structures of EGFR with inhibitors **2** and **4** bound within the EGFR active site. We expressed, purified and crystallized the kinase domain of human EGFR (amino acids 696–1,022) as previously described²¹; soaking these crystals overnight in a solution of either **2** or **4** afforded the cocrystal complexes. These crystals belong to space group *I*23 and show packing that is nearly identical to that of the crystals we recently described for reversible inhibitors bound to the EGFR kinase domain (**Supplementary Table 2** online)²¹. We solved both complex structures (EGFR–**2** and EGFR–**4**) by molecular replacement and refined them to 2.95 Å and 3.10 Å, respectively (**Supplementary Table 2**). The overall fold of these EGFR complexes is similar to those reported for the EGFR kinase

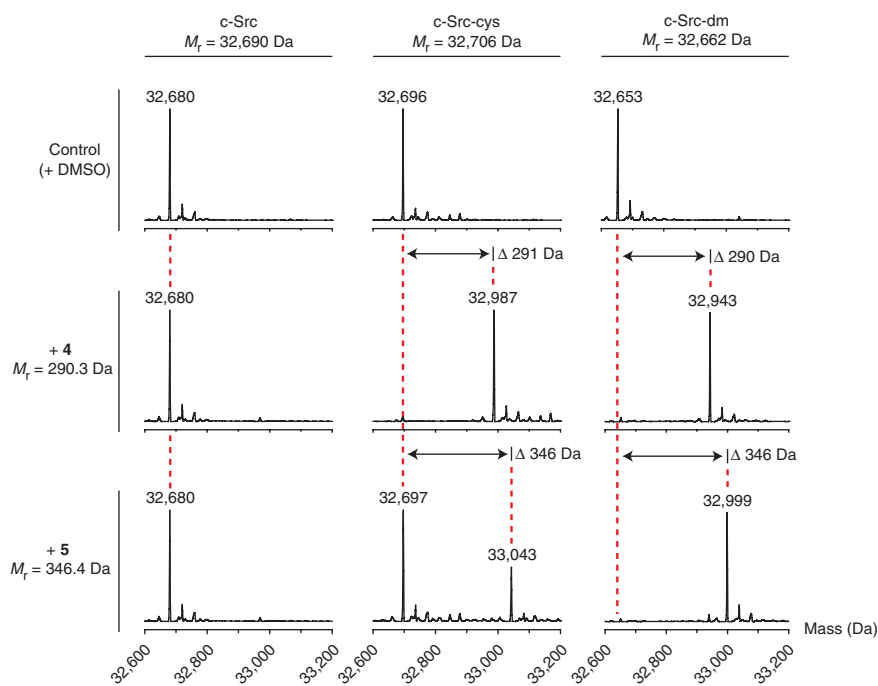


Figure 3 Deconvoluted mass spectra of c-Src variants treated with irreversible inhibitors suggest covalent inhibitor binding to kinase active sites bearing a properly positioned cysteine. ESI-*oa*-TOF of control and drug-treated c-Src kinases are shown. Note that c-Src-cys treated with **5** led to only ~30% conversion to the inhibitor-kinase adduct, whereas c-Src-cys and c-Src-dm treated with **4** and c-Src-dm treated with **5** resulted in stoichiometric adduct formation.

domain in an active conformation either in complex with reversible inhibitors or without ligand. The conserved salt bridge between Glu762 and the catalytic Lys745, which aligns the helix C in an active conformation, remains intact, which confirms the active conformation of these complexes^{16,21}. Both structures show nearly continuous electron density along the entire length of the protein, though some density is disordered around the C-terminal tail; therefore, we did not model in the refinement residues 986 and 990–1,005 in the EGFR–**4** complex, or 992–1,001 in EGFR–**2**.

The binding mode of EGFR–**2** and EGFR–**4**

The structures of EGFR in complex with **2** and **4** demonstrate that the inhibitors are bound covalently to Cys797 in the active site and adopt an orientation similar to that found for several kinases in complex with reversible quinazoline inhibitors (Fig. 4 and Supplementary Fig. 1 online). Clear electron density of the inhibitors and Cys797 shows formation of a new bond between the β -carbon atom of the acrylamide Michael acceptor on each inhibitor and the γ -sulfur atom of Cys797. These orientations within the EGFR active site are similar to those previously reported for reversible 4-anilinoquinazolines in complex with the kinases EGFR, CDK2, p38 MAPK, Aurora A and c-Src^{16,20–24}; both **2** and **4** form a hydrogen bond from the quinazoline N1 to the main chain amide of Met793 along the hinge region, and the C4 aniline points into the hydrophobic pocket defined by the gate-keeper, Thr790 (Fig. 4a and Supplementary Fig. 1). This key hydrogen bonding interaction provides substantial binding energy for reversible 4-anilinoquinazoline inhibitors; a carbon substitution of N1 results in ~3,700-fold loss of inhibitor potency in EGFR²⁵. Many kinase inhibitors form two hydrogen bonding interactions to the hinge region, and weak electron density may place a water molecule near the quinazoline N3 that represents a second, water-mediated hydrogen

bond to either Thr845 or Thr790. If present, this is likely a minor interaction, as loss of this interaction was reported for the co-crystal complex of EGFR with gefitinib (**14**), a potent reversible quinazoline inhibitor^{21,25}. We found an interplanar angle between the C4 aniline and the quinazoline core of ~45° for both inhibitors, and both aniline substituents were found to lie within 4 Å of the residue side chains comprising the hydrophobic selectivity pocket: Thr790, Leu788, Met766, Lys745, Glu762 and Thr854 (the *m*-bromine of **2** lies 3.4 Å away from Thr790, and the phenyl ring of **4** is 3.6 Å from Thr790).

Despite a similar overall binding mode, there are several differences between these structures and the previously published structure of the reversible inhibitor erlotinib in complex with EGFR¹⁶. In our EGFR cocystal structures, inhibitors **2** and **4** bind further away from the hinge region, and the quinazoline core of **2** and **4** tilts ~30° 'down' toward the C-terminal domain relative to erlotinib, pivoting about the hydrogen bond between N1 and the Met793 amide (Fig. 5a). These movements presumably allow covalent attachment between the inhibitor's acrylamide moiety and Cys797.

Complex structures of a target cysteine-containing c-Src mutant

To understand how covalent 6-acrylamido-4-anilinoquinazoline inhibitors exploit the cysteine specificity element in a kinase that does not naturally contain this cysteine, we solved cocystal structures of a cysteine-containing chicken c-Src mutant with inhibitors **2** and **4**. We carried out cocrystallization experiments by incubating the kinase domain of c-Src-cys (amino acids 251–533) with an excess of either **2** or **4** and removing insoluble material by centrifugation. The complex crystals (c-Src-cys–**2** and c-Src-cys–**4**) formed by hanging-drop vapor diffusion and belong to space group *P1*, which is the same space group reported previously for the human c-Src kinase domain²⁶. We solved both the complexes by molecular replacement with two monomers (A and B) of c-Src-cys in the crystallographic asymmetric unit and refined them to 2.48 Å and 2.50 Å, respectively (Supplementary Table 2). The overall fold of the chicken c-Src kinase domain mutant is similar to that of the wild-type human c-Src recently observed in an active conformation^{26,27}. The two molecules in the asymmetric unit differ slightly in areas of known flexibility and show weak or discontinuous main chain electron density for the N terminus (residues 251–254), the glycine-rich loop (residues 274–279), the helix C and connecting loop to β -strand 3 (residues 300–317) and the activation loop (residues 405–424) past the DFG motif. A detailed discussion of differences in the kinase conformation and inhibitor occupancy of the two molecules in the asymmetric unit is found in the Supplementary Note online.

The binding mode of c-Src-cys–**2** and c-Src-cys–**4**

The cocystals of c-Src-cys in complex with inhibitors **2** and **4** show covalent inhibitor binding to the kinase active site, and, as found in the EGFR–**2** and EGFR–**4** complexes, they reveal the inhibitors displaced from the predicted position based on reversible quinazoline

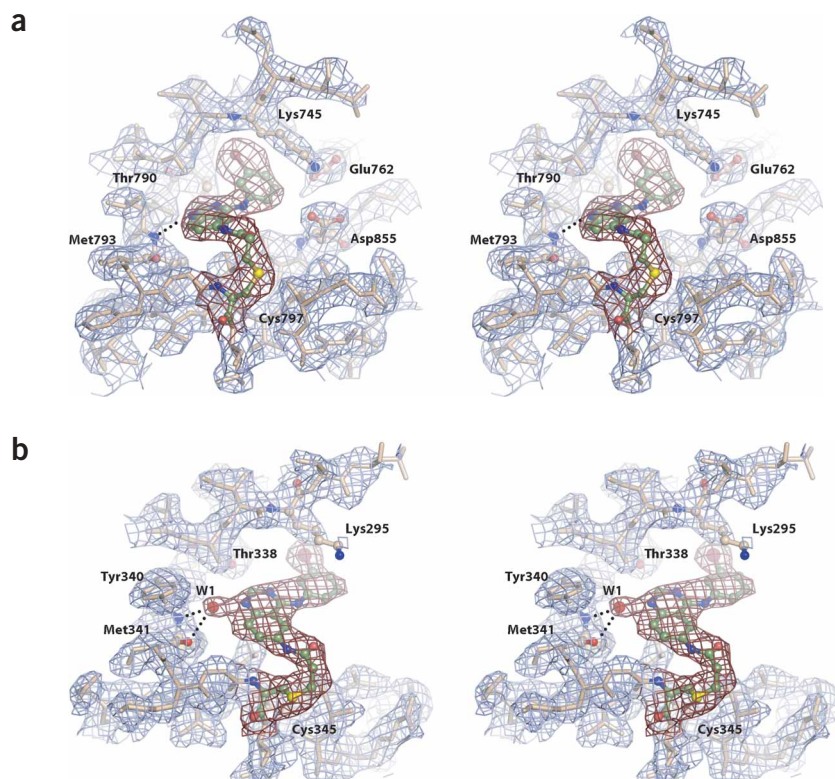


Figure 4 Stereodiagrams for irreversible 6-acrylamido-4-anilinoquinazoline inhibitor **2** covalently bound to the ATP site of both EGFR and c-Src-cys show different binding modes for each kinase. The experimental electron densities of EGFR and c-Src-cys at 2.95 Å and 2.48 Å resolution, respectively, are shown ($2F_o - F_c$ map contoured at 1σ). (a) Optimized EGFR inhibitor **2** (PD 168393)¹³ (green ball and sticks) in complex with the EGFR kinase domain shows clear electron density between the targeted Cys797 and the acrylamide Michael acceptor on **2**. The inhibitor makes a direct hydrogen bond between its quinazoline N1 and the main chain amide of Met793, which is a common recognition motif among reversible anilinoquinazolines and several protein kinase domains^{16,20–24}. We find the cocrystal complex in an active conformation of EGFR: a conserved salt bridge found only in active EGFR conformations between the catalytic Lys745 and helix C Glu762 remains intact. The *m*-bromine group sits adjacent (within 3.4 Å) to the gatekeeper residue, Thr790. (b) Notably, structures of **2** in complex with c-Src-cys show an inhibitor binding mode distinct from any reported for anilinoquinazolines with a protein kinase. In molecule B of the c-Src-cys–**2** complex, **2** (green ball and sticks) forms a water-mediated (W1) hydrogen bond via its N1 of the quinazoline core to the backbone amide of Met341.

binding¹⁸. As in the EGFR complexes described above, clear electron density defines covalent inhibitor binding to the engineered Cys345 (Fig. 4b and Supplementary Fig. 1). In contrast to the EGFR structures, however, the inhibitors in the c-Src-cys structures do not simply rotate with respect to the plane of the quinazoline but also make a substantial movement away from the hinge region with no direct hydrogen bonding contacts, and the C4 aniline substituents are coplanar with the quinazoline core (Figs. 4b and 5b; Supplementary Fig. 1). Furthermore, the individual conformations of the covalent c-Src-cys–inhibitor adducts (Cys345–**2** and Cys345–**4**) differ with respect to rotation around the C1–C2 bond of the former Michael acceptor system (dihedral 20°), consequently placing the inhibitor core of **2** even farther away from the hinge region, with the *m*-bromoaniline moiety stacked above Asp404 of the DFG motif and the side chain of the catalytic Lys295. In molecule B of

c-Src-cys–**2**, we observed one key hydrogen bond between the ligand and the backbone of the adenine binding pocket. The contact occurs through a water molecule (W1) that mediates a hydrogen bonding interaction between N1 (2.5 Å) of the quinazoline core and the backbone amide of Met341 (2.9 Å) of the hinge region (Fig. 4b). The same water molecule is found as W1027 coordinated to the backbone amide of Met341 in c-Src when neither ligand nor ATP is present^{26,28}. A similar water-mediated contact of a ligand to a structurally analogous backbone amide has recently been described for a new class of triaminotriazine-based p38 MAP kinase inhibitors²⁹.

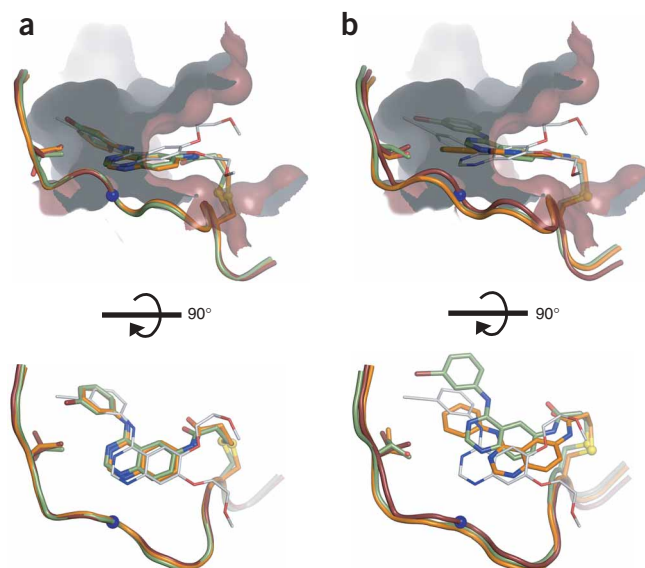


Figure 5 Comparison of the binding modes of **2** and **4** in EGFR and c-Src-cys with a canonical kinase–quinazoline binding mode reveals inhibitor movements necessary to accommodate covalent attachment. The crystal structures reported here aligned along the hinge-region residues (red loop) of the EGFR–erlotinib cocrystal (PDB entry 1M17; ref. 16). Erlotinib is shown as thin white sticks, **2** is shown as green sticks and **4** is shown as orange sticks. The covalently modified cysteine atoms are drawn as yellow spheres. (a) EGFR–**2** (green loop) and EGFR–**4** (orange loop) complexes compared with erlotinib. In the top panel, the irreversibly bound inhibitors rotate roughly 30° downward about the N1–backbone amide (blue sphere, Met793) hydrogen bond to accommodate covalent attachment to Cys797. The bottom panel illustrates the significant overlap of the irreversibly bound quinazoline core to the reversible inhibitor and reveals the close proximity of the C4 aniline substituents to the gatekeeper residue. (b) c-Src-cys–**2** (green loop) and c-Src-cys–**4** (orange loop) complexes compared with erlotinib. The irreversibly bound inhibitors bind farther away from the hinge region than erlotinib; no direct hydrogen bonding contacts are made.

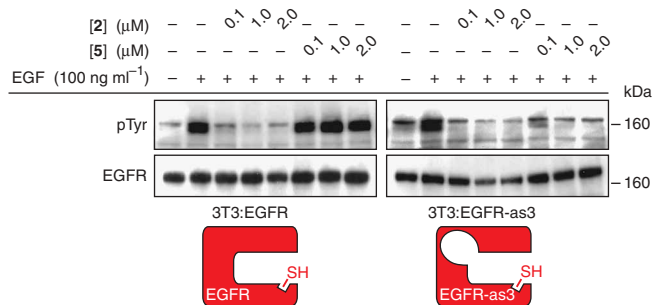


Figure 6 Reversal of tyrosine phosphorylation in cells demonstrates both the cell permeability and allele selectivity of two rationally designed 6-acrylamido-4-anilinoquinazoline inhibitors. NIH-3T3 cells transfected with EGFR or EGFR-as3 (3T3:EGFR and 3T3:EGFR-as3, respectively) were incubated with inhibitors **2** and **5** overnight before receptor stimulation with EGF. Immunoblots of the SDS-PAGE-separated cell lysates are shown. As expected, **2**, an EGFR-selective inhibitor¹³, reversed all EGF-dependent phosphotyrosine (pTyr) signals near 170 kDa, the approximate mass of EGFR. This phosphotyrosine signal was insensitive to cell treatment with as-allele-selective inhibitor **5** (left panel). Conversely, in the background of the analog-sensitive EGFR mutant 3T3:EGFR-as3, **5** was equipotent with **2**, reversing the EGF-stimulated phosphotyrosine to background levels (right panel).

Attempts to crystallize the double mutant c-Src-dm with the as-allele-selective inhibitor **5** produced ambiguous results (data not shown). For detailed discussion see the **Supplementary Note**. A model of the potential selectivity mechanism afforded by a gatekeeper mutation is illustrated in **Supplementary Figure 2** online.

5 inhibits analog-sensitive, but not wild-type, EGFR

To determine whether our rationally designed PD 168393 analogs were truly selective for kinases containing both specificity elements, we investigated whether **2** or **5** could inhibit EGFR—presumably the most stringent test, as wild-type EGFR contains the targeted cysteine residue and a threonine gatekeeper, and several reversible 4-anilinoquinazolines are highly potent EGFR inhibitors^{24,30–32}. Our *in vitro* screening data of irreversible inhibitors **2**, **4** and **5** tested against recombinant EGFR kinase affirm the conclusions from our c-Src-cys and Fyn-cys inhibition data: **5** is only weakly potent ($IC_{50} = 0.689 \mu\text{M}$) in the context of the targeted cysteine and a threonine gatekeeper (**Supplementary Table 3** online). Likewise, the cellular potency of these inhibitors matches the *in vitro* inhibitor selectivity profiles. We transfected NIH-3T3 cells, which have undetectable concentrations of endogenous EGFR, with either EGFR or EGFR-as3, an analog-sensitive allele of EGFR³³. In 3T3:EGFR cells treated with **2** then stimulated with EGF (100 ng ml^{-1}), we observed, as expected, complete inhibition of EGF-stimulated tyrosine phosphorylation

(**Fig. 6**). Under the same conditions, as-allele-selective inhibitor **5** did not inhibit the phosphotyrosine signal. In 3T3:EGFR-as3 cells (the analog-sensitive allele background), both **2** and **5** completely inhibited EGF-stimulated tyrosine phosphorylation. These results are consistent with the *in vitro* inhibition data of **5** against c-Src-dm (**Fig. 2b**), thus corroborating this inhibitor's selectivity for analog-sensitive kinase alleles with a targeted cysteine residue. Importantly, these data suggest that we can selectively target a designed double-mutant kinase with molecules such as **5** in the presence of wild-type EGFR.

Design and synthesis of a fluorescent affinity probe

We used structural analysis of the complex structures of EGFR and c-Src-cys with irreversible inhibitors **2** and **4** to identify a suitable site for attachment of a fluorophore to the 4-anilinoquinazoline scaffold without disrupting inhibitor potency. The C7 position of the quinazoline points outside the ATP binding pocket toward solvent (**Fig. 4**) and has been successfully modified to include solubilizing elements for otherwise poorly soluble quinazoline inhibitors³⁴. In addition, a recent report described a photoaffinity probe for EGFR (AX7593, **15**) that bears a tetramethylrhodamine fluorophore linked to a reversible 4-anilinoquinazoline inhibitor scaffold at the C7 position⁶. Based on these precedents, we functionalized the 6-acrylamido-4-anilinoquinazoline scaffold at C7 by tethering a fluorophore via a PEG linker, thereby forming the irreversible fluorescent probe **16** (**Fig. 7a** and

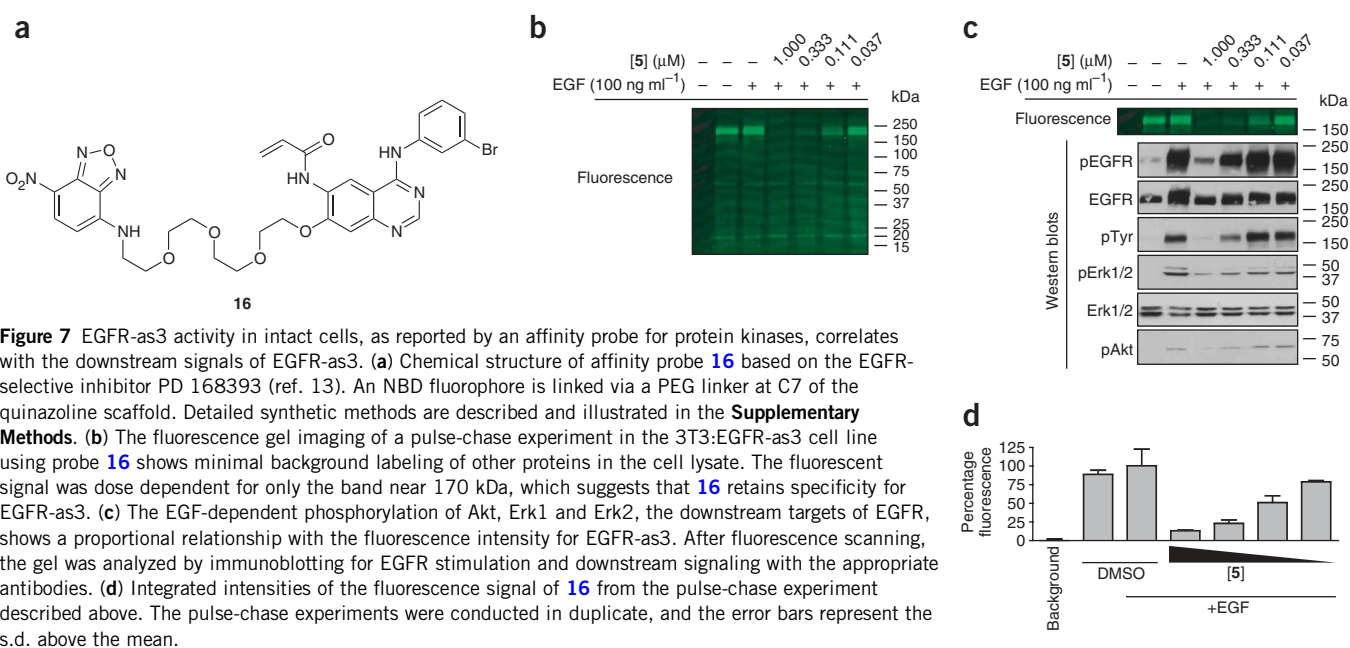


Figure 7 EGFR-as3 activity in intact cells, as reported by an affinity probe for protein kinases, correlates with the downstream signals of EGFR-as3. **(a)** Chemical structure of affinity probe **16** based on the EGFR-selective inhibitor PD 168393 (ref. 13). An NBD fluorophore is linked via a PEG linker at C7 of the quinazoline scaffold. Detailed synthetic methods are described and illustrated in the **Supplementary Methods**. **(b)** The fluorescence gel imaging of a pulse-chase experiment in the 3T3:EGFR-as3 cell line using probe **16** shows minimal background labeling of other proteins in the cell lysate. The fluorescent signal was dose dependent for only the band near 170 kDa, which suggests that **16** retains specificity for EGFR-as3. **(c)** The EGF-dependent phosphorylation of Akt, Erk1 and Erk2, the downstream targets of EGFR, shows a proportional relationship with the fluorescence intensity for EGFR-as3. After fluorescence scanning, the gel was analyzed by immunoblotting for EGFR stimulation and downstream signaling with the appropriate antibodies. **(d)** Integrated intensities of the fluorescence signal of **16** from the pulse-chase experiment described above. The pulse-chase experiments were conducted in duplicate, and the error bars represent the s.d. above the mean.

Supplementary Methods). To synthesize affinity probe **16**, we reacted an amine precursor with a fluorogenic benzofurazan reagent (NBD-Cl, **17**). Amine-linked NBD derivatives show environmentally sensitive fluorescence with both a hypsochromic shift of the emission spectra and an increase in fluorescence intensity upon binding to protein surfaces^{35,36}. Detailed synthetic procedures are described in **Supplementary Methods**. Affinity probe **16** has good water solubility, and we anticipated it to be selective for EGFR-family kinases because of its *m*-bromoaniline substituent¹³.

EGFR-as3 activity correlates with downstream signaling

To determine the requirement for EGFR-as3 activity in NIH-3T3 cells, we used affinity probe **16** in a pulse-chase experiment involving receptor stimulation with EGF. After treating serum-starved 3T3:EGFR-as3 cells with **5** for 90 min, we stimulated the cells with EGF (100 ng ml⁻¹) and then washed and treated the cells with 30 μM **16** for 25 min. Fluorescence imaging of the SDS-PAGE-separated lysates revealed minimal background labeling with a band near 170 kDa, which is consistent with the molecular weight of full-length EGFR-as3 (Fig. 7b). The signal was dose dependent with respect to the concentration of **5** added to the cells, and we observed strong maximal signals for the DMSO-treated controls. Furthermore, this fluorescence tracks with the amount of phospho-EGFR at each inhibitor concentration, which suggests that in the case of EGFR, activation of this pathway correlates linearly with active site occupancy.

Next, we sought to determine the relationship between activation of EGFR and activation of its downstream effectors. Stimulation of EGFR results in activating phosphorylation events on both the PI(3)K and the Ras/MAPK signaling pathways within cells³⁷. Immunoblotting for phospho-Akt (Ser473), phospho-Erk1 (Thr202) and phospho-Erk2 (Tyr204) (Fig. 7c) revealed activation proportional to both the phospho-EGFR signal and the fluorescence signal (the activity readout) (Fig. 7d). Thus, we find that the strength of a downstream signal is directly proportional to the percentage of available kinase active sites in the case of EGFR-as3.

DISCUSSION

The success of our chemical genetic design rested on the significant structural information available for 4-anilinoquinazoline inhibitors in complex with several kinases^{16,20–24}. These cocrystal structures revealed that C4 anilines extend into the hydrophobic pocket surrounding the gatekeeper residue. To exploit this feature, we explored the chemical space of the 6-acrylamido-4-anilinoquinazoline scaffold and defined the SAR necessary to achieve the best selectivity for the rationally designed double mutants c-Src-dm and Fyn-dm. As predicted based on reversible quinazoline inhibitors, a bulky C4 aniline was necessary to target kinases c-Src-as1, c-Src-dm, Fyn-as1 and Fyn-dm. Additionally, inhibitors bearing a 6-acrylamide substituent proved significantly more potent; the cysteine residue acts as a selectivity filter in a manner similar to that of an endogenous cysteine used to achieve selectivity for halomethylketone-containing pyrrolopyrimidines in RSK-family kinases¹⁵. Our *in vitro* and cellular experiments validate the structure-based chemical genetic design, which suggests that we can rationally target a kinase of interest for irreversible inhibition.

The close proximity of the C4 aniline groups of **2** and **4** to the gatekeeper in EGFR, as seen in the complex structures we report here, provides a structural explanation for the as-allele selectivity of bulky inhibitors such as **5**. The EGFR-**2** and EGFR-**4** complexes show C4 aniline moieties oriented adjacent to the gatekeeper residue and several residues comprising the hydrophobic pocket. In this

orientation, the pocket does not have enough volume to allow binding of significantly larger aniline substituents—an observation that underscores the importance of the gatekeeper's size in controlling inhibitor access to this pocket, which is essential for inhibitor potency. Upon mutation of the threonine gatekeeper to glycine, additional space permits larger aniline substituents to bind. Previously, we confirmed the basis of this selectivity mechanism in a cocrystal structure of inactive, full-length c-Src-as1 (T338G) in complex with *N*⁶-benzyl-ADP (**18**), an as-allele-selective ATP analog, and we found the benzyl ring to be within 3.5 Å of the glycine α-carbon³⁸. Thus, for compounds such as **5** that show greater selectivity for as-alleles, the scaffold binds deeper into the hydrophobic cleft made accessible by the glycine gatekeeper, thereby facilitating the interaction of the C4 aniline with the hydrophobic residues. The size and geometry of the C4 aniline is critical for the selectivity of these compounds, and the 6-acrylamide affords both increased potency and a chemical handle to the target cysteine-containing kinases.

Unexpectedly, the drug-sensitized c-Src structures in complex with PD 168393 analogs have an inhibitor binding mode that is different from predicted binding modes based on known reversible quinazolines. Crystal structures of reversible 4-anilinoquinazoline inhibitors bound to CDK2, p38 MAPK, Aurora A and EGFR kinases show similar binding modes, which suggests a common binding orientation of the scaffold among all kinases^{16,21–24}; we find this inhibitor orientation in our EGFR-**2** and EGFR-**4** complexes. Here, the key hydrogen bond between the quinazoline N1 and the backbone amide is maintained with only minor scaffold movements to accommodate the covalent attachment. Modeling of both reversible and irreversible 4-anilinoquinazolines into EGFR places the quinazoline scaffold in a similar orientation^{18,39}, which our EGFR complex structures confirm. In addition, a recently reported structure of c-Src in complex with AZD0530 (**19**), a potent, highly selective 5,7-disubstituted 4-anilinoquinazoline reversible inhibitor of c-Src and Abl, showed the key hydrogen bond between N1 and the Met341 main chain amide²⁰. Notably, our c-Src-cys structures reveal binding modes that do not make this conserved hydrogen bond but instead place the inhibitor away from the hinge region, toward the modified cysteine.

Based on these data, we believe that this class of irreversible inhibitor adopts two binding orientations within the kinase: a reversible binding mode necessary for inhibitor recognition and a shifted binding orientation necessary for covalent attachment. The SAR data from our panel of inhibitors suggest that inhibitor selectivity depends on essential contacts to the hinge region (for example, contacting the gatekeeper residue). In addition, the covalently modified EGFR and c-Src-cys structures show varying degrees of inhibitor mobility that enable covalent bond formation. Considering these results, we believe that perfect optimization of the reversible binding mode of the quinazoline scaffold is not an absolute requirement with irreversible inhibitors—the reversible interaction only needs to be strong enough to orient the acrylamide substituent in the vicinity of the target cysteine, where thermal motion allows covalent attachment between the inhibitor and the cysteine residue. The unexpected mobility of the inhibitor within the confines of the ATP binding pocket that we have observed is likely the basis for successful extension of this chemical genetic approach to irreversible kinase inhibition of three tyrosine kinases, despite the need for contacts with two disparate elements of the ATP binding site, which may vary from kinase to kinase.

The mobility of quinazoline-based irreversible inhibitors within kinase active sites, as suggested by our c-Src-cys structures, may explain the potency of irreversible inhibitors against emerging EGFR-driven cancers that are resistant to reversible anilinoquinazoline

inhibitor therapy. Two reversible quinazoline-based drugs, erlotinib and gefitinib, show clinical activity in non-small-cell lung cancers driven by EGFR, yet patients develop drug resistance through selection for mutations in the drug binding site of EGFR^{40–43}. Particularly troublesome for treatment of these cancers is a methionine mutation at the EGFR gatekeeper (T790M) that confers resistance to inhibition by erlotinib and gefitinib; this often results in relapse in people who once responded to drug treatment^{42,43}. Roughly half of all relapse patients harbor T790M^{42,43}, and emerging evidence using highly sensitive sequencing techniques suggests that T790M EGFR mutants exist in minor, barely detectable populations in pretreated cancers, which implies that reversible inhibitor treatment selects for these resistant cells over time until the treatment cannot overcome a critical population of cancer cells^{44,45}. Notably, several irreversible anilino-quinazoline-based inhibitors of EGFR show potency in cell culture against cells harboring the T790M mutation^{42,44,46–48}, which suggests that one mechanism for combating these resistant mutants is through irreversible inhibition, which we believe allows effective inhibition despite occlusion of the analogous reversible agents. In light of the recent discovery of minor populations of T790M EGFR conferring resistance, irreversible inhibitors may represent the best first-line treatments for non-small-cell lung cancers, or they may be effective in treating people who become resistant to the current first-line therapy. Future structural studies in the T790M background will likely identify the relevant inhibitor binding mode and may lead to optimized inhibitors that are able to combat drug resistance.

The irreversible inhibitors and fluorescent affinity probe **16** presented here represent a new set of chemical genetic tools that enable the quantitative analysis of the functional consequences of irreversibly inhibiting protein kinase activity. Using the fluorescent reporting functionality of **16**, we demonstrate that there is a linear correspondence between inhibition of EGFR kinase activity and inhibition of its downstream effectors. Although our current data are not of sufficient resolution to determine the exact quantitative relationship between EGFR and downstream effector activation, this experiment demonstrates that it may now be possible to directly test hypotheses regarding the thresholds of kinase activity necessary for signal propagation in other pathways.

METHODS

Generation and expression of c-Src mutants. We used the following reagents: the chicken c-Src (residues 251–533) gene cloned into pSKB-3 (a pET-28a vector (Novagen) modified to yield an N-terminal, tobacco etch virus protease-cleavable (His)₆ tag¹⁹), a plasmid containing tyrosine phosphatase YopH cloned into pCDFDuet-1 (Novagen)¹⁹, and a plasmid containing the chaperones GroEL and trigger factor cloned into pACYADuet-1 (Novagen). We used QuikChange mutagenesis (Stratagene) on the c-Src-containing plasmid to generate c-Src-as1 (T338G), c-Src-cys (S345C) and c-Src-dm (T338G S345C). We expressed and purified the c-Src mutants as previously described¹⁹, except we triply transformed the BL21 (DE3) *Escherichia coli* cells with c-Src, YopH, GroEL and trigger factor plasmids and additionally used chloramphenicol (34 µg ml⁻¹) during expression for the selection of GroEL and trigger factor. The expression yielded 2–10 mg of purified kinase per liter of bacterial culture. The concentration of the c-Src mutants was determined by absorbance spectroscopy at 280 nm using the calculated extinction coefficient of 52,370 M⁻¹ cm⁻¹. We concentrated the purified c-Src mutants to 15–18 mg ml⁻¹ and used them directly for structural studies. We froze the remaining c-Src kinase in liquid nitrogen, storing the aliquots at –80 °C for later use in biochemical assays.

In vitro kinase assays for c-Src variants. We performed radioactive phospho-transfer assays in triplicate at various inhibitor concentrations as reported previously¹⁰. Details of the assay are described in **Supplementary Methods**.

Mass spectrometry of c-Src variants. We used the purified kinase domains (residues 251–533) of three c-Src variants for MS experiments. To 5 µg of c-Src, c-Src-cys or c-Src-dm in 10 µl of buffer (50 mM Tris (pH 8.0), 100 mM NaCl, 5% (v/v) glycerol, 1 mM DTT) we added 3 µl of DMSO, **4** or **5** (100 µM in DMSO). We incubated this mixture (23 µM:15 µM inhibitor/kinase; 1.5:1 molar equivalents) on ice for 15 min and then diluted it into 100 µl water. We analyzed aliquots (20 µl) by mass spectrometry using an HTS PAL 12-plate autosampler (CTC Analytics) and an LCT Premier XE LC-ESI-oe-TOF mass spectrometer (Waters).

Generation and expression of EGFR for structural studies. The expression and purification of EGFR was similar to methods we recently described²¹. We describe the detailed methods in **Supplementary Methods**.

Crystallization and data collection of EGFR-2 and EGFR-4. We obtained crystals by the hanging-drop vapor diffusion method (precipitant: 1.2 M potassium sodium tartrate, 0.1 M HEPES (pH 7.5), 5 mM Tris(2-carboxyethyl)phosphine hydrochloride) and made complex crystals by soaking crystals overnight in a solution containing 400 µM of either inhibitor **2** or **4**. We collected diffraction data at Argonne National Laboratory Advanced Photon Source, beamline ID24, under a nitrogen gas stream at 100 K, using a wavelength of 0.9795 nm. We processed the data with HKL2000 and DENZO/SCALEPACK⁴⁹.

Structure determination and refinement of EGFR-2 and EGFR-4. We solved the EGFR by molecular replacement with starting coordinates from an isomorphous EGFR structure (Protein Data Bank (PDB) entry 1M17; ref. 16). We describe the details of the structure determination and refinement in **Supplementary Methods**. Detailed data and refinement statistics are given in **Supplementary Table 2**. We produced the figures using PyMOL⁵⁰. Ramachandran statistics are shown in **Supplementary Table 4** online.

Crystallization and data collection of c-Src-cys-2 and c-Src-cys-4. We expressed and purified the chicken c-Src-cys variant as described above, and we describe the formation of the cocrystals in **Supplementary Methods**. We used a cryoprotectant of 20% glycerol before flash freezing the crystals in liquid nitrogen. We collected the diffraction data at the Berkeley Lab Advanced Light Source, beamlines 8.2.1 and 8.2.2, under a nitrogen gas stream at 100 K, using a wavelength of 1.0000 nm. We processed the data with DENZO and SCALEPACK⁴⁹ using HKL2000.

Structure determination and refinement of c-Src-cys-2 and c-Src-cys-4. We solved the chicken c-Src-cys (S345C) structures by molecular replacement with starting coordinates from the catalytic domain of human c-Src (PDB entry 1Y0J; ref. 26). Further determination and refinement details are available online (**Supplementary Methods**). We present detailed data and refinement statistics in **Supplementary Table 2**. We used PyMOL⁵⁰ to produce the figures. Ramachandran statistics are shown in **Supplementary Table 4**.

Cell culture, retrovirus production and infection. We previously described establishing 3T3:EGFR (ref. 33). Similarly, we transduced NIH-3T3 cells with EGFR-as3, an analog-sensitive allele of EGFR kinase; the construction of EGFR-as3 is described in the **Supplementary Methods**. We cultured the NIH-3T3 cells in DMEM supplemented with 10% FBS (FBS) and a solution of penicillin 'G' (100 units ml⁻¹) and streptomycin sulfate (100 µg ml⁻¹) (PenStrep, University of California, San Francisco Cell Culture Facility). To produce ecotropic virus, we transfected EGFR-as3 (cloned into pWZLhygro vector) into Bosc23 cells. We selected pools of transduced rodent fibroblasts by adding hygromycin (Roche) at 48 h; this selection lasted 2 weeks using hygromycin 500 µg ml⁻¹.

Reversal of tyrosine phosphorylation in 3T3:EGFR and 3T3:EGFR-as3 cells. We incubated either EGFR-transduced cells or EGFR-as3-transduced cells with control (1.2% DMSO) or with drug (0.1 µM, 1.0 µM and 2.0 µM inhibitors **2** or **5**, 1.2% DMSO) and treated the cells with or without EGF (100 ng ml⁻¹, Roche) for 30 min before harvest. After 3 h of incubation, we lysed the cells using Upstate lysis buffer (Upstate), separated equal amounts of total protein using 4–12% SDS-PAGE and transferred the gel to nitrocellulose membranes. We immunoblotted the membranes with antibodies against phosphotyrosine (4G10, Upstate Biotechnology; 1:500) or EGFR (Ab5, NeoMarkers; 1:2,000)

and detected the antibodies with horseradish peroxidase-conjugated sheep antibody to mouse (Amersham Pharmacia Biotech), followed by enhanced chemiluminescence (Amersham Pharmacia Biotech).

Measurement of EGFR-as3 activity and its downstream signals *in vivo*. We serum-starved 3T3:EGFR-as3 cells overnight in DMEM supplemented with 0.5% FBS and PenStrep. The next day, we treated the cells with medium (DMEM plus 0.5% FBS and PenStrep) containing either 1% DMSO or 1% DMSO with three-fold dilutions of **5** from 1 μ M to 37 nM. After a 1.5-h inhibitor treatment, we stimulated the cells for 10 min with EGF (100 ng ml⁻¹, Sigma), placed the dishes on ice, washed the cells with cold (0–4 °C, ice-bath-chilled) phosphate-buffered saline and incubated them with 30 μ M fluorescent affinity probe **16** in cold phosphate-buffered saline for 25 min. We then lysed the cells, normalized the lysates for protein content and separated the lysates using SDS-PAGE. We scanned the gels on a flat-bed fluorescence imager (Typhoon, Molecular Dynamics) and then transferred them to nitrocellulose for immunoblot analysis. We measured the fluorescence intensity using ImageQuant software (Molecular Dynamics). We performed the cell treatments in duplicate. See **Supplementary Methods** for additional details.

Accession codes. Protein Data Bank: coordinates and structure factors from this study have been deposited under accession codes 2J5E, 2J5F, 2HWO and 2HWP. Structures cited from previous studies include 1M17 and 1YOJ.

Note: Supplementary information and chemical compound information is available on the Nature Chemical Biology website.

ACKNOWLEDGMENTS

We thank E. Garner and R.D. Mullins (University of California, San Francisco) and the J.A. Wells lab (University of California, San Francisco) for reagents and use of instrumentation. We thank M. Seeliger and J. Kuriyan (University of California, Berkeley) for the plasmid containing the chicken c-Src gene, the plasmid containing tyrosine phosphatase YopH, and the purified c-Src kinase domain. We thank G. Montelione (Rutgers) for the plasmid containing GroEL and trigger factor. We thank J. Taunton, T. Hirano, D. Maly and R. Bateman for assistance with organic synthesis and data collection, and Q. Justman, M. Feldman, A. Dar and B. Olson for helpful comments on the manuscript. We thank the staff and funding agencies of beamlines 8.2.1 and 8.2.2 (Advanced Light Source) and beamline ID24 (Argonne National Laboratory Advanced Photon Source) for their assistance with X-ray diffraction data collection. This work was supported in part by US National Institutes of Health grants A144009 (K.M.S.), CA080942 (M.J.E.), CA116020 (M.J.E.), NCRN RR015804 and NCRN RR001614 (NIH Resource to University of California, San Francisco) and by the Sandler Program in Basic Sciences (K.M.S. and W.A.W.) and the Burroughs Wellcome Fund (W.A.W.). M.J.E. is the recipient of a Scholar Award from the Leukemia and Lymphoma Society.

AUTHOR CONTRIBUTIONS

J.A.B. and C.K. synthesized the panel of inhibitors, expressed the Fyn variants and measured the Fyn *in vitro* IC₅₀ values. J.A.B. and D.R. expressed the c-Src variants, crystallized and measured the c-Src-cys cocrystals and measured the EGFR-as3 cellular activity. J.A.B. conducted the protein mass spectrometry and measured the c-Src and EGFR *in vitro* IC₅₀ values. D.R. and H.R. synthesized and characterized probe **16**. D.R. solved the c-Src-cys complex structures. Q.W.F. established the 3T3:EGFR cell lines and conducted the cellular inhibition experiments with **2** and **5**. C.H.Y. expressed, crystallized and solved the EGFR complex structures. J.A.B. prepared the manuscript, with help from and editing by all the co-authors. C.Z. conceptualized the initial chemical genetic design. W.A.W., M.J.E. and K.M.S. helped conceive of experiments.

COMPETING INTERESTS STATEMENT

The authors declare no competing financial interests.

Published online at <http://www.nature.com/naturechemicalbiology>

Reprints and permissions information is available online at <http://npg.nature.com/reprintsandpermissions>

- Cohen, P. Protein kinases—the major drug targets of the twenty-first century? *Nat. Rev. Drug Discov.* **1**, 309–315 (2002).
- Knight, Z.A. & Shokat, K.M. Features of selective kinase inhibitors. *Chem. Biol.* **12**, 621–637 (2005).

- Kung, C., Kenski, D.M., Krukenberg, K., Madhani, H.D. & Shokat, K.M. Selective kinase inhibition by exploiting differential pathway sensitivity. *Chem. Biol.* **13**, 399–407 (2006).
- Ventura, J.J. *et al.* Chemical genetic analysis of the time course of signal transduction by JNK. *Mol. Cell* **21**, 701–710 (2006).
- Evans, M.J. & Cravatt, B.F. Mechanism-based profiling of enzyme families. *Chem. Rev.* **106**, 3279–3301 (2006).
- Shreder, K.R., Wong, M.S., Nomanbhoy, T., Leventhal, P.S. & Fuller, S.R. Synthesis of AX7593, a quinazoline-derived photoaffinity probe for EGFR. *Org. Lett.* **6**, 3715–3718 (2004).
- Yee, M.C., Fas, S.C., Stohlmeyer, M.M., Wandless, T.J. & Cimprich, K.A. A cell-permeable, activity-based probe for protein and lipid kinases. *J. Biol. Chem.* **280**, 29053–29059 (2005).
- Yuan, H. *et al.* Synthesis and activity of C11-modified wortmannin probes for PI3 kinase. *Bioconjug. Chem.* **16**, 669–675 (2005).
- Liu, Y. *et al.* Wortmannin, a widely used phosphoinositide 3-kinase inhibitor, also potently inhibits mammalian polo-like kinase. *Chem. Biol.* **12**, 99–107 (2005).
- Liu, Y. *et al.* Structural basis for selective inhibition of Src family kinases by PP1. *Chem. Biol.* **6**, 671–678 (1999).
- Buzko, O. & Shokat, K.M. A kinase sequence database: sequence alignments and family assignment. *Bioinformatics* **18**, 1274–1275 (2002).
- Bishop, A.C. *et al.* A chemical switch for inhibitor-sensitive alleles of any protein kinase. *Nature* **407**, 395–401 (2000).
- Fry, D.W. *et al.* Specific, irreversible inactivation of the epidermal growth factor receptor and erbB2, by a new class of tyrosine kinase inhibitor. *Proc. Natl. Acad. Sci. USA* **95**, 12022–12027 (1998).
- Singh, J. *et al.* Structure-based design of a potent, selective, and irreversible inhibitor of the catalytic domain of the erbB receptor subfamily of protein tyrosine kinases. *J. Med. Chem.* **40**, 1130–1135 (1997).
- Cohen, M.S., Zhang, C., Shokat, K.M. & Taunton, J. Structural bioinformatics-based design of selective, irreversible kinase inhibitors. *Science* **308**, 1318–1321 (2005).
- Stamos, J., Sliwkowski, M.X. & Eigenbrot, C. Structure of the epidermal growth factor receptor kinase domain alone and in complex with a 4-anilinoquinazoline inhibitor. *J. Biol. Chem.* **277**, 46265–46272 (2002).
- Fan, Q.W., Zhang, C., Shokat, K.M. & Weiss, W.A. Chemical genetic blockade of transformation reveals dependence on aberrant oncogenic signaling. *Curr. Biol.* **12**, 1386–1394 (2002).
- Tsou, H.R. *et al.* 6-Substituted-4-(3-bromophenylamino)quinazolines as putative irreversible inhibitors of the epidermal growth factor receptor (EGFR) and human epidermal growth factor receptor (HER-2) tyrosine kinases with enhanced antitumor activity. *J. Med. Chem.* **44**, 2719–2734 (2001).
- Seeliger, M.A. *et al.* High yield bacterial expression of active c-Abl and c-Src tyrosine kinases. *Protein Sci.* **14**, 3135–3139 (2005).
- Hennequin, L.F. *et al.* N-(5-chloro-1,3-benzodioxol-4-yl)-7-[2-(4-methylpiperazin-1-yl)ethoxy]-5-(tetrahydro-2H-pyran-4-yloxy)quinazolin-4-amine, a novel, highly selective, orally available, dual-specific c-Src/Abl kinase inhibitor. *J. Med. Chem.* **49**, 6465–6488 (2006).
- Yun, C.-H. *et al.* Structures of lung cancer-derived EGFR mutants and inhibitor complexes: mechanism of activation and insights into differential inhibitor sensitivity. *Cancer Cell* (in the press).
- Heron, N.M. *et al.* SAR and inhibitor complex structure determination of a novel class of potent and specific Aurora kinase inhibitors. *Bioorg. Med. Chem. Lett.* **16**, 1320–1323 (2006).
- Shewchuk, L. *et al.* Binding mode of the 4-anilinoquinazoline class of protein kinase inhibitor: X-ray crystallographic studies of 4-anilinoquinazolines bound to cyclin-dependent kinase 2 and p38 kinase. *J. Med. Chem.* **43**, 133–138 (2000).
- Wood, E.R. *et al.* A unique structure for epidermal growth factor receptor bound to GW572016 (lapatinib): relationships among protein conformation, inhibitor off-rate, and receptor activity in tumor cells. *Cancer Res.* **64**, 6652–6659 (2004).
- Fry, D.W. Mechanism of action of erbB tyrosine kinase inhibitors. *Exp. Cell Res.* **284**, 131–139 (2003).
- Breitenlechner, C.B. *et al.* Crystal structures of active SRC kinase domain complexes. *J. Mol. Biol.* **353**, 222–231 (2005).
- Cowan-Jacob, S.W. *et al.* The crystal structure of a c-Src complex in an active conformation suggests possible steps in c-Src activation. *Structure* **13**, 861–871 (2005).
- Xu, W., Harrison, S.C. & Eck, M.J. Three-dimensional structure of the tyrosine kinase c-Src. *Nature* **385**, 595–602 (1997).
- Leftheris, K. *et al.* The discovery of orally active triaminotriazine aniline amides as inhibitors of p38 MAP kinase. *J. Med. Chem.* **47**, 6283–6291 (2004).
- Fry, D.W. *et al.* A specific inhibitor of the epidermal growth factor receptor tyrosine kinase. *Science* **265**, 1093–1095 (1994).
- Pollack, V.A. *et al.* Inhibition of epidermal growth factor receptor-associated tyrosine phosphorylation in human carcinomas with CP-358,774: dynamics of receptor inhibition *in situ* and antitumor effects in athymic mice. *J. Pharmacol. Exp. Ther.* **291**, 739–748 (1999).
- Wakeling, A.E. *et al.* ZD1839 (Iressa): an orally active inhibitor of epidermal growth factor signaling with potential for cancer therapy. *Cancer Res.* **62**, 5749–5754 (2002).
- Fan, Q.W. *et al.* Combinatorial efficacy achieved through two-point blockade within a signaling pathway—a chemical genetic approach. *Cancer Res.* **63**, 8930–8938 (2003).
- Small, J.B. *et al.* Tyrosine kinase inhibitors. 17. Irreversible inhibitors of the epidermal growth factor receptor: 4-(phenylamino)quinazoline- and 4-(phenylamino)pyrido[3,

- 2-d]pyrimidine-6-acrylamides bearing additional solubilizing functions. *J. Med. Chem.* **43**, 1380–1397 (2000).
35. Rasmussen, S.G. *et al.* Biophysical characterization of the cocaine binding pocket in the serotonin transporter using a fluorescent cocaine analogue as a molecular reporter. *J. Biol. Chem.* **276**, 4717–4723 (2001).
36. Uchiyama, S., Santa, T., Okiyama, N., Fukushima, T. & Imai, K. Fluorogenic and fluorescent labeling reagents with a benzofurazan skeleton. *Biomed. Chromatogr.* **15**, 295–318 (2001).
37. Jorissen, R.N. *et al.* Epidermal growth factor receptor: mechanisms of activation and signalling. *Exp. Cell Res.* **284**, 31–53 (2003).
38. Witucki, L.A. *et al.* Mutant tyrosine kinases with unnatural nucleotide specificity retain the structure and phospho-acceptor specificity of the wild-type enzyme. *Chem. Biol.* **9**, 25–33 (2002).
39. Wissner, A. *et al.* 4-Anilino-6,7-dialkoxyquinoline-3-carbonitrile inhibitors of epidermal growth factor receptor kinase and their bioisosteric relationship to the 4-anilino-6,7-dialkoxyquinazoline inhibitors. *J. Med. Chem.* **43**, 3244–3256 (2000).
40. Lynch, T.J. *et al.* Activating mutations in the epidermal growth factor receptor underlying responsiveness of non-small-cell lung cancer to gefitinib. *N. Engl. J. Med.* **350**, 2129–2139 (2004).
41. Paez, J.G. *et al.* EGFR mutations in lung cancer: correlation with clinical response to gefitinib therapy. *Science* **304**, 1497–1500 (2004).
42. Kobayashi, S. *et al.* EGFR mutation and resistance of non-small-cell lung cancer to gefitinib. *N. Engl. J. Med.* **352**, 786–792 (2005).
43. Pao, W. *et al.* Acquired resistance of lung adenocarcinomas to gefitinib or erlotinib is associated with a second mutation in the EGFR kinase domain. *PLoS Med.* **2**, e73 (2005).
44. Engelman, J.A. *et al.* Allelic dilution obscures detection of a biologically significant resistance mutation in EGFR-amplified lung cancer. *J. Clin. Invest.* **116**, 2695–2706 (2006).
45. Inukai, M. *et al.* Presence of epidermal growth factor receptor gene T790M mutation as a minor clone in non-small cell lung cancer. *Cancer Res.* **66**, 7854–7858 (2006).
46. Carter, T.A. *et al.* Inhibition of drug-resistant mutants of ABL, KIT, and EGF receptor kinases. *Proc. Natl. Acad. Sci. USA* **102**, 11011–11016 (2005).
47. Kobayashi, S. *et al.* An alternative inhibitor overcomes resistance caused by a mutation of the epidermal growth factor receptor. *Cancer Res.* **65**, 7096–7101 (2005).
48. Kwak, E.L. *et al.* Irreversible inhibitors of the EGF receptor may circumvent acquired resistance to gefitinib. *Proc. Natl. Acad. Sci. USA* **102**, 7665–7670 (2005).
49. Otwinowski, Z. & Minor, W. Processing of X-ray diffraction data collected in oscillation mode. *Methods Enzymol.* **276**, 307–326 (1997).
50. DeLano, W.L. *The PyMOL Molecular Graphics System* (DeLano Scientific, San Carlos, California, USA, 2002).